China Steel Technical Report, No. 34, pp.34－39, (2021)

Development of High-Performance Silicon-Carbon Composite Anode for Rechargeable Lithium-Ion Batteries

CHENG-HSIEN YANG and KAI-HSUAN HUNG

New Materials Research & Development Department
China Steel Corporation

With a view to the anodes in a lithium-ion battery, the promising silicon owns the advantage of higher theoretical capacity (3579-4200 mAh/g), which is ten times higher than that of conventional graphite. However, the volume expansion caused by Li-Si alloying reaction leads to silicon particle pulverization and rapid cell failure. In this study, the mechanical grinding technique was adopted to produce ~50-nm silicon powder, which is below the proposed critical size for non particle cracking. Nevertheless, the increasing surface area of silicon nanoparticles results in excessive solid electrolyte interface (SEI) and reduced electrochemical performance. Accordingly, the pitch-derived carbon coating for stable SEI is another significant process. The core-shell Si-C composites with various silicon sources, pitches and their mixing ratios are discussed. The outstanding Si-C composite features ~50-nm silicon powder coated with a specific pitch-derived carbon. According to the half-cell assembly (CR2032 type) and tests, this optimum composite contributes a discharge capacity as high as 1987 mAh/g for its first delithiation, and retained 80% capacity after 45 charge-discharge cycles, which outperformed the benchmark products.

Keywords: lithium-ion battery, silicon, pitch, nanosizing, electrochemical performance.

1. INTRODUCTION

Rechargeable lithium-ion batteries have successfully penetrated consumer markets mainly based on high energy densities and other balanced electrochemical properties[1,2], the energy densities available with conventional electrode materials has almost reach saturation. In view of anode, graphite theoretically can store only one lithium ion per six carbons (LiC_6), corresponding to a gravimetric capacity of 372 mAh/g. In an effort to further increase the specific capacity, the promising silicon owns the advantages of high theoretical capacity (3579-4200 mAh/g for $Li_{3.75}Si$-$Li_{4.4}Si$) as well as low operation voltage (0.4 V vs. Li/Li^+), abundant resources (the second most in the earth's crust), and environmental benignity (non-toxic). Furthermore, the semiconductor industry can sufficiently supply the raw silicon with low cost. Therefore, Si is recognized as one of the most potential anode materials to replace the existing graphitic anode materials in the near future[3].

During the charge-discharge process, however, the pure silicon forms lithium-silicon alloy, causing volume expansion nearly three times as much[4]. The stress caused by the repeated volume expansion and contraction leads to the silicon particle pulverization, electrode disintegration, and eventual rapid cell failure. In order to prolong the life of the electrode, nanosizing silicon particles down to below 150 nm was proposed to alleviate expansion-driven stress and pulverization[5]. In this work, the mechanical grinding method was adopted to achieve industrial mass production. Moreover, wet grinding ensures safe and effective manufacture. Considering efficient grinding, a multi-step process using different sizes of ceramic beads are often carried out. Large grinding beads take advantage of the high grinding efficiency. On the other hand, small grinding beads help to obtain the target particle size.

Grinding silicon powders to nanometric size can alleviate the volume expansion/contraction caused by lithium alloying/dealloying, and inhibit its rapid cracking and cell failure. Nevertheless, the increasing surface area of silicon nanoparticles causes more irreversible side reactions in contact with electrolyte during the charge-discharge process, resulting in excessive solid electrolyte interface (SEI) and reduced first-cycle coulombic efficiency and cycle stability. Common enhancement strategies include silicon surface coating and secondary particle size modification. Among them, the carbonaceous material has a small volume change and good cyclic stability during charge-discharge. When a core-shell silicon/carbon structure is fabricated, the above-mentioned irreversible reactions will be greatly suppressed. This SEI stabilization method was adopted as the significant second step.

2. EXPERIMENTAL METHOD

2.1 Preparation of Silicon-Carbon Composite

The raw materials included micrometric silicon powders and pitches, the former were commercially purchased, which were purified from the silicon wafer-sawing waste, the latter were refined from coal tar oil by China Steel Chemical Corporation (CSCC). The scraps sources ensured low cost, stable supply, and circular economy. To obtain ~50-nm silicon powders, the micrometric silicon powders were introduced to a bead mill system. Pitches were heated close to its softening temperature before mixing with silicon nanopowders to achieve a homogeneous composite. The following calcination caused loss of low-molecular-weight volatiles, polymerization and finally carbonization of pitches. Silicon-carbon composite was thus obtained.

2.2 Materials Characterizations and Electrochemistry

High-resolution transmission electron microscopy (TEM; JEOL 2100F) was used to examine the silicon nanoparticles. The morphologies of as-prepared Si-C powders and electrodes were inspected using a focused ion beam system (SEM; FEI Helios NanoLab G3 CX).

To prepare the electrode, an aqueous slurry made of 92 wt% active material powder (CSCC graphite and Si-based powders), 8 wt% of conductive carbon, and binder was mixed using agitator and then pasted onto Cu foil. This electrode was vacuum-dried at 110°C for 8 h, roll-pressed, and then punched to match the required dimensions of a CR2032 coin cell. The active material loading amount was typically 5.5-6.0 mg cm^{-2}. Li foil and a glass fiber membrane were used as the counter electrode and separator, respectively. 1 M $LiPF_6$ in EC/DEC/EMC electrolyte were received from Formosa Plastics Corporation. The assembly of the coin cells were performed in an argon-filled glove box (MBraun, MB10), where both the moisture content and oxygen content were maintained at below 1 ppm. The charge–discharge performance (such as capacity, coulombic efficiency, and cyclic stability) of the Si-containing electrodes was evaluated using a battery tester (Arbin, BT-2043).

3. RESULTS AND DISCUSSION

3.1 Preparation of Silicon-Carbon Composite

After rough and fine grinding of the micrometric silicon powders, the TEM images of the as-milled Si nanoparticles are shown in Figure 1. The rough grinding stage can reduce the silicon particle size to hundreds of nanometers (540 minutes elapsed). The following fine grinding stage can further reduce the particle size of most silicon powders to 50~100 nm (additional 120 minutes elapsed), and some silicon powders were even ground to below 50 nm, which met the preset expectation. The specific energy of the equipment was the comprehensive index including the grinding parameters such as spindle speed, the grinding bead size, and the filling amount of the grinding beads, etc., which was suitable for normalizing the various grinding batches and determining the grinding termination. Thus, the correlation of the grinding specific energy and the silicon particle size (D_{50} or D_{90} measured by particle size analyzer) is shown in Figure 2. The particle size analyzer featured immediacy and statistics. The results showed that the median (D_{50}) size of the silicon particles is below 150 nm (critical size without expansion-driven pulverization) when the specific energy surpassed 30 Wh/g. With increasing the specific energy to 40 Wh/g, D_{50} and D_{90} of the silicon particles almost reached their limits, namely 105 and 180 nm, respectively. An effective process to fabricate 50~100-nm silicon powders was readily established.

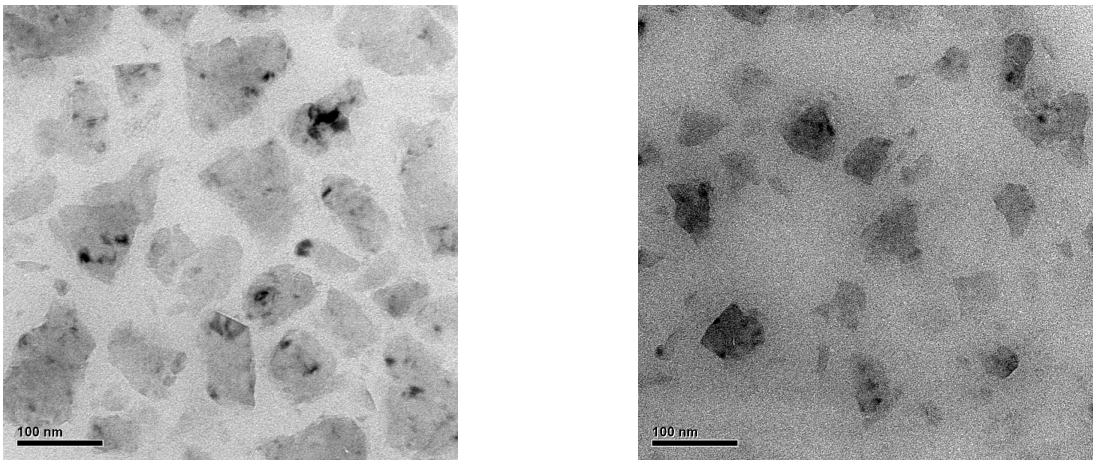

(a) (b)

Fig.1. TEM images of the as-milled silicon nanoparticles after (a) rough and (b) fine grinding.

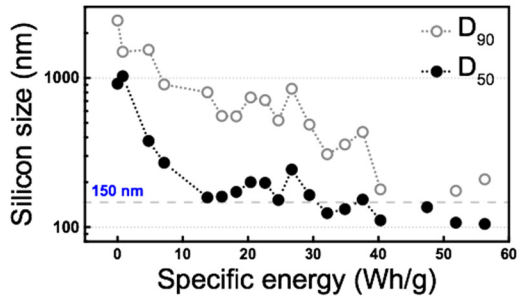

Fig.2. The correlation of the grinding specific energy and the silicon particle size.

Pitch coating, high-temperature carbonization, and pulverization processes were then carried out for fabricating Si-C composite. SEM images of Si-C composite powders are shown in Figure 3. As shown in Figure 3(a), the size of Si-C composite powders was generally in the range of 1~20 μm. The cross-sectional SEM image of the single Si-C particle, prepared by a focused ion beam, demonstrated hundreds of silicon nanoparticles were encapsulated by the pitch-derived carbon. Thus, a core-shell Si-C structure is fabricated.

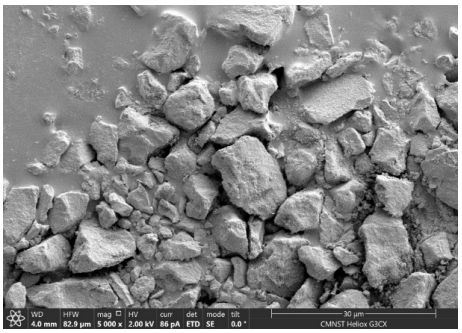

(a)

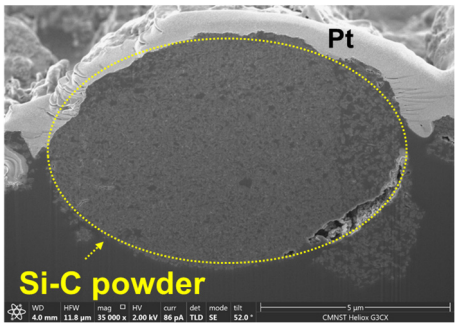

(b)

Fig.3. (a) Plane view and (b) cross-section SEM image of Si-C composite powders.

3.2 Electrochemical Performance of Silicon-Carbon Composite Anode

The first charge–discharge profiles of the silicon-based material/graphite anodes are shown in Figure 4. As shown, the delithiation potential plateau between 0.1 and 0.25 V was characteristic of lithium de-intercalation from graphite, which was the main constituent for all anodes. The first charge–discharge profile of pure graphite anode demonstrated the discharge capacity of 367 mAh/g. When the potential rose to 0.25~0.5 V, the capacity of the silicon-based material/graphite anode increased significantly, attributed to the dealloying reaction of silicon. Besides, the lithiation potential of the anode containing Si-C was higher than that containing SiOx, which indicated lower lithiation overpotential and impedance of the former anode due to its surface conductive carbon layer. The fabricated Si-C composite was expected to be beneficial to the fast charging performance.

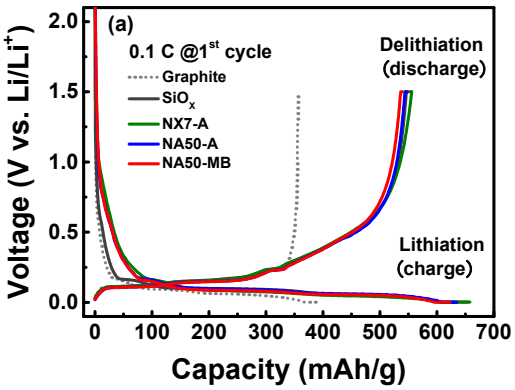

Fig.4. Charge–discharge curves at 0.1C (55 mA g^{-1}) of the various Si-based material/graphite anodes measured with 1 M $LiPF_6$ in EC/DEC/EMC electrolyte at 25°C.

The silicon sources, pitches, and their mixing ratios affected the electrochemical performance of the Si-containing anode. The test results of the anodes containing the various Si-based materials are listed in Table 1. To fairly compare the cyclic stability of the various anodes, the first discharge capacity of all anodes was normalized to 550 mAh/g by adjusting the amount of the Si-based materials in anodes. As shown, the ~50-nm silicon powders coated by pitch A, namely NA50-A, contributed 1926 mAh/g for its first discharge reaction as shown in Table 1, which was much higher than 1665 mAh/g for NX7-A and 1712 for SiOx. The former was made of commercially available ~80-nm silicon powders and the same carbon coating process. The latter was a SiOx benchmark product made by Japanese manufacturer. The higher capacity of NA50-A was ascribed to its smaller silicon size and the outer conductive carbon layer. Furthermore, pitch A was replaced by a lower-softening-temperature pitch (namely pitch B) to improve its fluidity and enable a uniform and thin carbon coating layer after carbonization. Therefore, the as-prepared

Table 1 Electrochemical properties of Si-based materials/graphite anodes.

Active materials	First charge capacity of anode (mAh/g)	First discharge capacity of anode (mAh/g)	First charge capacity of Si-based materials (mAh/g)	First discharge capacity of Si-based materials (mAh/g)	First cycle efficiency of anode (%)	Cycle stability of anode (cycle, ≧ 80% capacity retention)
NX7-A/graphite	614	539	1980	1665	88	32
NA50-A/graphite	636	546	2414	1926	86	31
NA50-LB/graphite	615	539	2432	2030	88	24
NA50-MB/graphite	625	541	2456	1987	87	45
NA50-HB/graphite	629	551	1936	1622	88	33
SiOx/graphite	647	555	2133	1712	86	33

Charge and discharge indicated lithiation and delithiation reactions, respectively.

NA50-MB contributed discharge capacity as high as 1987 mAh/g for its first delithiation, and retained 80% capacity after 45 charge-discharge cycles. Figure 5 shows cyclic stabilities at 0.5C (275 mA g^{-1}) of the various Si-C/graphite anodes. The capacity retention of the NA50-MB/graphite anode outperformed that of the others.

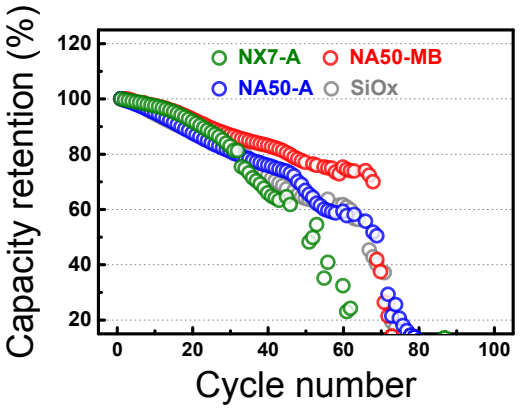

Fig.5. Cyclic stability at 0.5C (275 mA g^{-1}) of the various Si-based material/graphite anodes measured with 1 M $LiPF_6$ in EC/DEC/EMC electrolyte at 25°C.

By changing the ratio of pitch B to silicon nanopowders, the amount of the carbon layer was tuned to enhance electrochemical performance. Figure 6 shows cyclic stability at 0.5C (275 mA g^{-1}) of the various NA50-XB/graphite (X=L, M, H) anodes. If this ratio reduced, namely NA50-LB, the first discharge capacity increased to 2030 mAh/g. However, it retained 80% capacity after only 24 charge-discharge cycles. The cyclic stability compromised due to weak protection of the incomplete carbon coating. If the ratio increased, namely NA50-HB, the first discharge capacity reduced to 1622 mAh/g. It retained 80% capacity after 33 cycles. This can be explained by the longer lithium ion diffusion path, leading to the incomplete alloying reaction. And the high impedance easily caused the electrolyte decomposition and rapid capacity fading. In short, the anode containing NA50-MB performed the optimum electrochemistry.

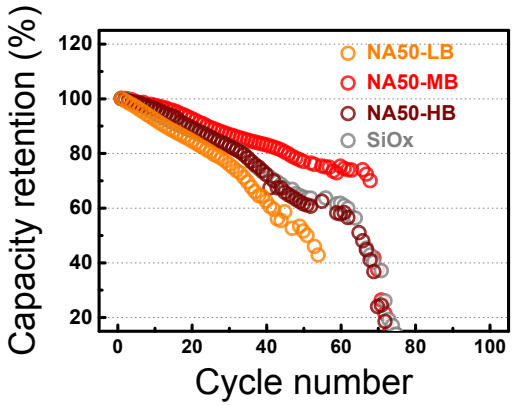

Fig.6. Cyclic stability at 0.5C (275 mA g^{-1}) of the Si-based material (with the various coated carbon amount)/graphite anodes measured with 1 M $LiPF_6$ in EC/DEC/EMC electrolyte at 25°C.

3.3 Failure Investigation of Silicon-Carbon Composite Anode

In order to understand the failure mechanism of the anode, the post-mortem anodes after 50 charge-discharge cycles were carefully taken out from the testing cell and washed by EMC solvent. A series of cross-section sample preparation processes enabling ion mill and focused ion beam were carried out. Figure 7 shows the cross-section SEM images of the (a) pristine and (b) post-mortem SiOx/graphite anodes. As shown, the

SiOx-containing anode expanded from ~43 μm (fresh anode excluding Cu current collector) to ~225 μm (cycled anode). In contrast, the NA50-MB/graphite anode only expanded from ~38 μm (fresh anode) to ~65 μm (cycled anode) as shown in Figure 8. The former expanded three times larger than the latter. A thick SEI layer formation on SiOx surface can be generally found for SiOx-containing anode. Earlier literatures[6] proposed that silicon oxide reacted with lithium to form electrochemically-irreversible lithium silicate and lithium oxide, causing low first-cycle charge–discharge coulombic efficiency. In contrast, a thin SEI layer on the intact Si-C particles were found for NA50-MB/graphite anode, benefiting less anode expansion, electrical contact between active materials or with the current collector, and also longer cyclic stability.

4. CONCLUSIONS

Based on the established silicon nanosizing and carbon coating techniques, the Si-C composite for the anode of lithium-ion battery can be fabricated. This study found the silicon, pitch, and their mixing ratio significantly affected the electrochemical performance of the Si-containing anode. The outstanding NA50-MB anode material was characteristic of ~50-nm silicon powders coated with a low-softening-temperature pitch-derived carbon. It contributed to a discharge capacity as high as 1987 mAh/g for its first delithiation, and retained 80% capacity after 45 charge–discharge cycles, which outperformed that of the commercial silicon powder and SiOx benchmark product. Moreover, the carbon coating amount was tuned to obtain the optimum discharge capacity and cyclic stability of Si-C anode material. Despite the superior electrochemical properties of the as-prepared Si-C composite employing the half-cell assembling (CR2032 coin type) and tests, it still needed to pass the full cell tests and approval (e.g. 18650 cylinder and pouch type) by the downstream cell manufacturers for practical use.

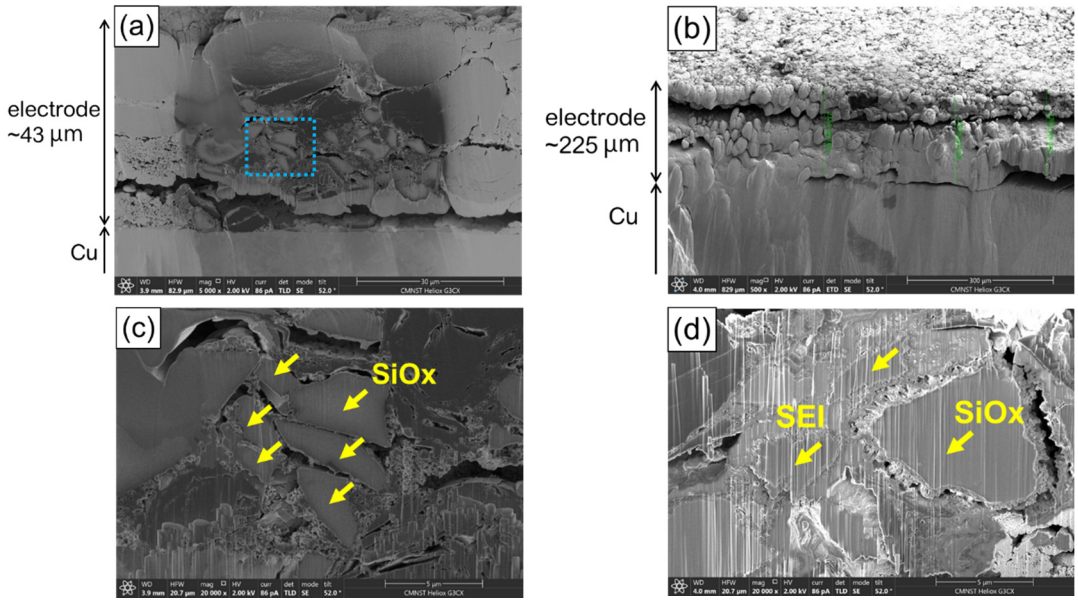

Fig.7. (a,b) Low- and (c,d) high-magnification cross-section SEM images of the (a,c) pristine and (b,d) post-mortem SiOx/graphite anodes.

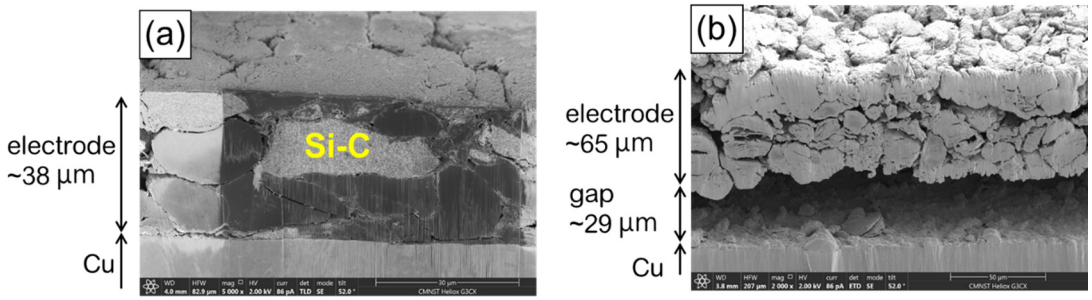

Fig.8. Cross-section SEM images of the (a) pristine and (b) post-mortem NA50-MB/graphite anodes.

REFERENCES

1. J. M. Tarascon and M. Armand: Nature, 2001, vol. 414, pp. 359-67.
2. J. W. Choi and D. Aurbach: Nat. Rev. Mater., 2016, vol. 1, 16013.
3. T. Kwon, J. W. Choi and A. Coskun: Chem. Soc. Rev., 2018, vol. 47, pp. 2145-64.
4. M. Ashuri, Q. He and L. L. Shaw: Nanoscale, 2016, vol. 8, pp. 74-103.
5. M. Gu, Y. He, J. Zheng and C. Wang: Nano Energy, 2015, vol. 17, pp. 366-83.
6. W. Luo, X. Chen, Y. Xia, M. Chen, L. Wang, Q. Wang, W. Li and J. Yang: Adv. Energy Mater., 2017, vol. 7, 1701083.